JOURNAL OF VIROLOGY, Nov. 2007, p. 12307–12315 Vol. 81, No. 22
0022-538X/07/$08.00+0 doi:10.1128/JVI.01002-07

Infection of Cardiomyocytes and Induction of Left Ventricle Dysfunction by Neurovirulent Polytropic Murine Retrovirus▽

Mohammed Khaleduzzaman,[1] Joseph Francis,[2] Meryll E. Corbin,[1] Elizabeth McIlwain,[2] Marc Boudreaux,[1] Min Du,[1] Tim W. Morgan, and Karin E. Peterson[1]*

Department of Pathobiological Sciences[1] and Department of Comparative Biomedical Sciences,[2] School of Veterinary Medicine, Louisiana State University, Skip Bertman Dr., Baton Rouge, Louisiana 70803

Received 8 May 2007/Accepted 3 September 2007

Viral infections of the heart are a causative factor of myocarditis as well as of sudden, unexpected deaths of children, yet the mechanisms of pathogenesis remain unclear, in part due to the relatively few animal models of virus-induced myocarditis. In the current study, we examined the ability of polytropic murine retroviruses to infect the heart and induce cardiac dysfunction. In situ hybridization and immunohistochemistry analysis detected virus-infected cardiomyocytes and macrophages in the heart. A significant decrease in left ventricle function, as measured by fractional shortening, was detected in mice infected with the neurovirulent retrovirus Fr98 but not in mice infected with the nonneurovirulent retrovirus Fr54. Virus infection was not associated with consistent findings of fibrosis or substantial cellular infiltrate. Fr98-induced left ventricle dysfunction was associated with a higher virus load, increased mRNA expression of the macrophage marker F4/80, increased chemokine production, and a small number of apoptotic cells in the heart.

Viruses, including Coxsackie virus, influenza virus, cytomegalovirus, hepatitis C virus, and human immunodeficiency virus, have been detected in the heart muscles of children with cardiovascular diseases and may play an important role in myocarditis as well as in sudden, unexpected deaths of children (6, 8, 15–17). Despite the detection of these viruses in the heart, the mechanisms by which these viruses contribute to cardiac disease remain unclear. In some cases, only minimal virus infection and diffuse regions of cellular infiltrate are associated with virus-associated heart disease (4, 8). Mechanisms such as the release of cytokines or the recruitment of inflammatory cells to the heart may contribute to cardiac damage. However, there are only a limited number of small-animal models of viral-induced myocarditis; these include Coxsackie B3 virus, the ecotropic retrovirus complex LP-BM5, and herpes virus infection in mice (2, 3, 7, 13).

In the current study, we investigated the use of murine polytropic retrovirus infection in mice as a model to study viral pathogenesis in the heart. The receptor for polytropic retroviruses is xenotropic/polytropic receptor 1 (XPR1) (37, 40). *Xpr1* mRNA was observed in heart tissue, suggesting that polytropic retroviruses may target and infect cells in the heart (37). Additionally, virus-infected macrophages may infiltrate the heart in a manner similar to what is observed with other viral infections (8, 39, 41). We compared the ability of two different polytropic viruses to induce cardiac dysfunction: Fr98, a highly neurovirulent retrovirus that induces neurological disease in mice, and Fr54, a nonneurovirulent retrovirus that replicates in the central nervous system at a lower level than Fr98 does (27). The neurological disease induced by Fr98 is characterized by ataxia, seizures, and death and is associated with a strong innate immune response in the central nervous system (25, 27). The primary difference between Fr98 and Fr54 is the envelope gene, although both viruses infect the same cell types, which include macrophages (27, 32).

An analysis of heart tissue from mice infected with either Fr98 or Fr54 showed virus-infected macrophages and cardiomyocytes, as detected by both in situ and immunohistochemistry analysis. Interestingly, pathogenesis in the heart correlated with neuropathogenesis, as the neurovirulent virus Fr98 induced left ventricular dysfunction, while the nonneurovirulent virus Fr54 did not induce detectable cardiac damage.

MATERIALS AND METHODS

Mice. All animal experiments were conducted with 129S6 (129SvEv) mice maintained at the Louisiana State University School of Veterinary Medicine and were carried out in accordance with the regulations of the Louisiana State University Animal Care and Use Committee and the guidelines of the NIH.

Virus infection of mice. The construction of virus clones Fr98 and Fr54 has been described previously (27). Virus stocks were prepared from the supernatants of confluent cultures of infected *Mus dunni* fibroblasts. Virus titers were determined by focus-forming assays using the envelope-specific monoclonal antibodies 514 and 720 (31). Mice were infected within 24 h of birth by intraperitoneal injection with 100 μl of cell culture supernatant containing 10^4 focus-forming units of Fr98, Fr54, or supernatant from mock-infected cells. Mice were observed daily for clinical signs, which were characterized by hyperexcitability for 2 to 3 days, starting around 14 to 21 days postinfection. This sign was followed by the onset of multiple seizures and then progressive development of ataxia and/or death within a 2-week period (9, 24). Some infected mice also showed signs of weight loss compared to littermates and uninfected controls.

Echocardiogram analysis. Echocardiography was performed using a Toshiba Aplio SSH770 (Toshiba Medical Systems, Tustin, CA) fitted with a PLT 1202 linear transducer (12 or 14 MHz), which generates two-dimensional images at frame rates ranging from 300 to 500 frames per second. Mice were ear tagged prior to analysis by echocardiogram, and the echocardiograms were performed and analyzed in a blind study. Prior to analysis, mice were anesthetized with Avertin (2.5% wt/vol, 8 μl/g, intraperitoneally). Each anterior chest was shaved, and acoustic gel was applied to the chest wall to enhance sound transduction. Images were obtained using a linear array probe at a center frequency of 14.0 MHz. Two-dimensional and M-mode echocardiographic measurements of the

* Corresponding author. Mailing address: Department of Pathobiological Sciences, School of Veterinary Medicine, Louisiana State University, Baton Rouge, LA 70803. Phone: (225) 578-9681. Fax: (225) 578-9701. E-mail: kpeterson@vetmed.lsu.edu.

▽ Published ahead of print on 12 September 2007.

TABLE 1. List of primers used for real-time PCR analysis

Common protein name	Gene (NCBI no.)	Forward primer	Reverse primer
Alpha-1 type I collagen	*Col1a1* (gi/12842)	GAGAGCATGACCGATGGATT	CCTTCTTGAGGTTGCCAGTC
Atrial natriuretic peptide (Anp)	*Nppa* (gi/230899)	GGAGGTCAACCCACCTCTG	GCTCCAATCCTGTCAATCCTAC
Brain natriuretic peptide (Bnp)	*Nppb* (gi/18158)	GAGGCGAGACAAGGGAGAA	TGCATCTTGAATTGCTCTGG
Chemokine ligand 4/MIP-1β (Ccl4)	*Ccl4* (gi/20303)	AGTCCCAGCTCTGTGCAAAC	CCACGAGCAAGAGGAGAGAG
Chemokine ligand 5/RANTES (Ccl5)	*Ccl5* (gi/20304)	GGTTTCTTGATTCTGACCCTGTA	AGGACCGGAGTGGGAGTAG
CD3 antigen, epsilon polypeptide (Cd3e)	*Cd3e* (gi/12501)	GAGCACCCTGCTACTCCTTG	TGAGCAGCCTGATTCTTTCA
Chemokine receptor 1 (Ccr1)	*Ccr1* (gi/1276)	TCAAAGCATGACCAGCATCTA	CTTGTAGTCAATCCAGAAAGG TAAA
Chemokine receptor 5 (Ccr5)	*Ccr5* (gi/12774)	CGAAAACACATGGTCAAACG	CCATTCCTACTCCCAAGCTG
Friend murine leukemia virus FB29 *gag* (*gag*)	*gag* (gi/1491876)	CCCGTGGCGGATTCTACT	TCGGAGAAAGAGGGGTTGTTA
F4/80	*Emr1* (gi/13733)	ACAAGTGTCTCCCTCGTGCT	AACATGGTGCTTTCCACAGTC
Glyceraldehyde-3-phosphate dehydrogenase (Gapdh)	*Gapdh* (gi/407972)	TGCACCACCAACTGCTTAGC	TGGATGCAGGGATGATGTTC
Interferon beta (Ifnb1)	*Ifnb1* (gi/15977)	AGCACTGGGTGGAATGAGAC	TCCCACGTCAATCTTTCCTC
Interferon gamma (Ifng)	*Ifng* (gi/15978)	CCATCGGCTGACCTAGAGAA	ATGAGGAAGAGCTGCAAAGC
Nitric oxide synthase 2 (iNos)	*Nos2* (gi/18126)	GACGGATAGGCAGAGATTGG	CACATGCAAGGAAGGGAACT
Tumor necrosis factor alpha (Tnf)	*Tnf* (gi/21926)	CCACCACGCTCTTCTGTCTAC	GAGGGTCTGGGCCATAGAA

interventricular septum, posterior wall, and left ventricle diameter (LVD) were recorded for the parasternal long-axis view of the left ventricle as well as for the parasternal short-axis view at the level of the papillary muscles. Ventricle dysfunction was measured by the percentage of fractional shortening (LVD diastole-LVD systole/LVD diastole), which determines the change in diameter of the left ventricle between contracted and relaxed states. All measurements were performed for three different cardiac cycles, and the values were averaged. The procedure lasted for less than 10 min, after which the mice were allowed to recover and returned to their cage.

Preparation of RNA for real-time PCR analysis. Infected mice and uninfected controls were exsanguinated by axillary incision under deep isoflurane anesthesia, followed by cervical dislocation. Brains and hearts were removed from infected mice at the time points indicated. Brain tissue was divided into two sections by midsagittal dissection. Hearts were placed in 0.9% saline or 1× phosphate-buffered saline (PBS), pH 7.0, for 2 to 5 min to pump out residual blood and were cut by cross-sectional division. Tissue sections were immediately frozen in liquid nitrogen and stored at −80°C or placed in 10% neutral buffered formalin and processed for histology. Total RNA from frozen tissue was prepared using TRIzol reagent (Invitrogen, Carlsbad, CA) according to the manufacturer's instructions. Total RNA for each sample was subsequently treated with DNase (Ambion, Austin, TX) for 30 min to remove any contaminating DNA and purified over Zymo RNA cleanup columns (Zymo Research, Orange, CA). RNA was reverse transcribed by using the iScript reverse transcription kit (Bio-Rad Laboratories, Hercules, CA) according to the manufacturer's instructions. The reverse transcription reaction was diluted fourfold in RNase-free water prior to use in quantitative real-time PCRs.

Quantitative real-time PCR analysis of gene expression. Primers for real-time PCR analysis are shown in Table 1 and were designed using Primer3 software (34). Primer pairs were blasted using the National Center for Biotechnology Information website to confirm specificity. Reactions were run in triplicate by using SYBR green mix with Rox (Bio-Rad) in a 10-μl volume with approximately 10 ng of cDNA and a final concentration of 1.8 μM of forward and reverse primers. Samples were run on an ABI PRISM 7900 sequence detection system (Applied Biosystems, Foster City, CA). Melting curve analysis demonstrated a single product for each primer pair. Lack of DNA contamination was confirmed by conducting reactions without reverse transcriptase; untranscribed controls either tested negative for all genes after 40 cycles or had an expression level at least a 1,000-fold lower than that of the analyzed samples. The cycle number at which each sample reached a fixed fluorescence threshold (C_T) was used to quantify gene expression. Data were calculated as the C_T value ($\log_2$) for *Gapdh* minus the C_T value of the gene of interest for each sample ($\Delta C_T = C_T$ *Gapdh* − C_T gene of interest) to account for variations in RNA in each sample. The data are presented as a percentage of *Gapdh* expression for each gene of interest.

Histological analysis. Histologic samples were immersion fixed in 10% neutral buffered formalin for a minimum of 24 h and then embedded in paraffin. These sections were adhered to a glass slide. Hematoxylin and eosin and trichrome stains of longitudinal sections and cross-sections of heart tissue were completed by an American Journal of Clinical Pathology-certified histology technician at the Louisiana State University School of Veterinary Medicine histology laboratory. The slides were examined by a board certified pathologist in a blind study.

Immunohistochemistry for virus, Iba1, XPR1, and desmin detection. Tissue sections incubated at room temperature (rt) for a minimum of 24 h in 10% neutral buffered formalin were processed for histology and embedded in paraffin; 4-μm sections were cut and placed on Superfrost slides. Slides were incubated overnight at 56°C to fix tissues. Slides were then placed in xylene for 15 min, followed by rehydration. Antigen retrieval was performed by incubating slides in 0.018 M citric acid, 8.2 uM sodium citrate dihydrate, pH 6.0, for 20 min at 120°C in a decloaking chamber (Biocare Medical, Concord, CA) at 12 to 15 lb/in^2 and cooled to 90°C. Following equilibration to rt, slides were incubated in 0.2% fish skin gelatin (FSG) (Sigma-Aldrich, St. Louis, MO) in PBS for 10 min. This solution was also used to wash slides between all incubations. Tissues were blocked in a humidity chamber for a minimum of 30 min with blocking solution consisting of 2% donkey serum (Sigma), 1% bovine serum albumin (BSA) (Sigma), 0.05% FSG, 0.1% Triton X-100 (Sigma), and 0.05% Tween 20 (Bio-Rad) in PBS. For the detection of virus-infected cells, slides were incubated overnight at 4°C with a 1/500 dilution of goat polyclonal anti-gp70 serum (32). For the detection of XPR1, slides were incubated with rabbit polyclonal anti-XPR1 (Imgenex, San Diego, CA). Slides were then incubated with 5 μg/ml of biotinylated rabbit anti-goat immunoglobulin G (IgG) or goat anti-rabbit IgG (Molecular Probes) for 30 min at rt and then incubated with 4 μg/ml of streptavidin conjugated to Alexa Fluor 594 (Invitrogen) or Alexa Fluor 488 for 30 min at rt. For dual staining or detection of macrophages, slides were incubated in blocking solution for 30 min, incubated with 2.5 μg/ml of rabbit polyclonal anti-Iba1 (Wako USA, Richmond, VA) in 0.2% FSG in PBS at 4°C overnight or 30 min at rt. For the detection of myocytes, sections were incubated with rabbit polyclonal anti-desmin (Abcam, Cambridge, MA). Slides were then incubated with 6.7 μg/ml Alexa Fluor 594- or Alexa Fluor 488-conjugated goat anti-rabbit IgG for 30 min at rt. Slides were counterstained with 100 ng/ml of 4′,6-diamidino-2-phenylindole (DAPI) (Molecular Probes) for 25 min. Slides were mounted with ProLong Gold antifade reagent (Molecular Probes) and allowed to set for at least 2 h at 4°C. The lack of nonspecific staining was confirmed using uninfected mice with the gp70 primary antibody as well as no primary antibody controls (data not shown).

Generation of probes for in situ hybridization. Approximately 1 μg of a plasmid containing a 200-bp fragment of the N-terminal region of the Fr98 envelope gene (plasmid 1579) was digested with EcoRI for 1 h, and diluted in 0.1× Tris-EDTA buffer, pH 8.0; enzymes were removed by phenol-chloroform extraction. DNA was precipitated using lithium chloride (0.4 M final concentration) and 100% ethanol. The DNA was resuspended in 0.1× Tris-EDTA buffer. Digoxigenin (DIG)-labeled sense and anti-sense probes were generated using the DIG RNA labeling kit (Roche Molecular Biochemicals, Indianapolis, IN), T7 polymerase, and 1 μg of linearized template DNA according to the manufacturer's instructions. DIG-labeled probes were purified over Zymo RNA cleanup columns. Probe concentration was calculated by limiting serial dilutions

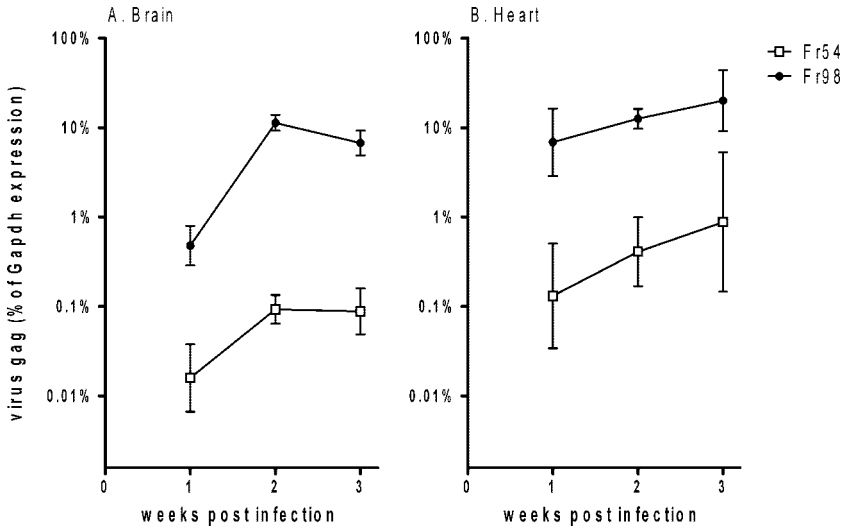

FIG. 1. Virus expression in (A) brain and (B) heart over 3 wpi in 129SvEv mice. Newborn mice were infected with 10^4 focus-forming units of Fr98 or Fr54 by intraperitoneal injection. Brain and heart tissue were removed from Fr98- and Fr54-infected mice at the indicated time. Virus *gag* RNA levels were determined using quantitative real-time PCR using SYBR green detection. The PCR product was sequenced to confirm the amplification of the correct gene. Data are expressed as virus mRNA levels as a percentage of *Gapdh* mRNA levels in each sample. Data are the means ± standard errors for four to eight samples per group per time point. Error bars indicate standard deviations.

of the probes on nylon membrane with comparison to a known standard (Roche Molecular Biochemicals).

In situ hybridization. In situ hybridization was performed as described previously (9, 23). DIG-labeled probes were detected with alkaline-phosphatase-labeled anti-DIG antibodies (Roche Molecular Biochemicals) by using the Fast-Red substrate (Roche Molecular Biochemicals). Sections were counterstained with hematoxylin. The specificity of the probe to Fr98/Fr54 virus was confirmed by the absence of staining in uninfected mice as well as by the use of nonspecific probes (Fig. 3A and data not shown).

Multiplex assay for chemokine expression. Heart tissue was removed from mice at 3 weeks postinfection (wpi). Hearts were placed in 0.9% saline or 1× PBS for 2 to 5 min to pump out residual blood and cut once by cross-sectional division. Tissue sections were immediately frozen in liquid nitrogen and stored at −80°C. To generate tissue homogenates for bead analysis, samples were homogenized in 200 μl of Bio-Plex cell lysis solution (Bio-Rad) containing complete mini protease inhibitors (Roche Molecular Biochemicals) and 2 mM phenylmethylsulfonyl fluoride (Sigma-Aldrich). Samples were homogenized using Kontes disposable pellet pestles (Fisher Scientific, Hampton, NH). Cellular debris was removed by centrifugation at 4,500 × *g* for 15 min at 4°C. Samples were analyzed for cytokine protein expression by using a Bio-Rad 6-plex Bio-Plex assay on a Bio-Plex instrument following the manufacturer's instructions and were calculated as picograms per milliliter by using a standard curve from in-plate standards before subsequently converting them to femtograms per milligram of brain tissue.

Apoptosis detection. Apoptotic cells were detected by using the CardioTACS apoptosis detection kit (R&D Research, Minneapolis MN) according to the manufacturer's instructions. The lack of nonspecific staining was confirmed by using uninfected mice as well as by using kit controls.

Statistical analysis. All statistical analysis described the figure legends was completed using GraphPad Prism software (GraphPad, San Diego, CA).

RESULTS

Comparison of virus RNA levels in heart and brain tissue. Analysis of virus replication in the brain and heart was detected by quantitative real-time reverse transcriptase PCR using primers to the *gag* gene, which is identical for Fr98 and Fr54. Fr98 RNA was readily detectable in the brains of 129SvEv mice at 1 wpi by quantitative real-time reverse transcriptase PCR, with a substantial increase in virus RNA levels at 2 wpi (Fig. 1A); prior to the onset of disease at 3 wpi, RNA of the nonneurovirulent retrovirus Fr54 was also detectable in the brain between 1 and 3 wpi, but at a substantially lower level compared to Fr98 (Fig. 1A). At 1 wpi, the level of virus RNA in both Fr98- and Fr54-infected mice was approximately a log higher in the heart than in the brain (Fig. 1A and B). However, at 2 and 3 wpi, virus levels were similar between the heart and brain. Fr54 virus RNA levels in the heart were substantially lower than Fr98 virus RNA levels in both the heart and brain (Fig. 1B). Thus, both Fr98 and Fr54 can infect heart tissue, but with different kinetics than those observed in the brain.

Virus infection of macrophages. We determined which cell types were infected in the heart by using immunohistochemical analysis for the virus envelope protein. Virus-infected cells were detected throughout the heart, with many positive cells located near blood vessels, suggesting the infiltration of virus-infected cells from the blood (Fig. 2A). Immunohistochemical analysis for the macrophage marker Iba1 confirmed the presence of macrophages around the blood vessels (Fig. 2B). Dual labeling with both Iba1 and virus envelope protein demonstrated that these macrophages were infected with virus (Fig. 2C).

Virus infection of myocytes. In addition to virus-positive macrophages, multiple cardiomyocytes were also positive for virus envelope in both Fr54- and Fr98-infected mice (Fig. 2E). Dual staining with gp70 and the myocyte-specific marker desmin confirmed the infection of myocytes by polytropic retrovirus (Fig. 2F). To determine whether myocytes were productively infected, we used in situ hybridization analysis to detect viral RNA. Viral RNA was detected in numerous cells of Fr98-infected mice (Fig. 3B). The probe did not cross-react with endogenous retroviral transcripts, as no signal was observed in uninfected or mock-treated animals (Fig. 3A). Virus RNA expression was observed in myocytes (Fig. 3C) in numerous areas in the heart. Interestingly, some of the virus-positive

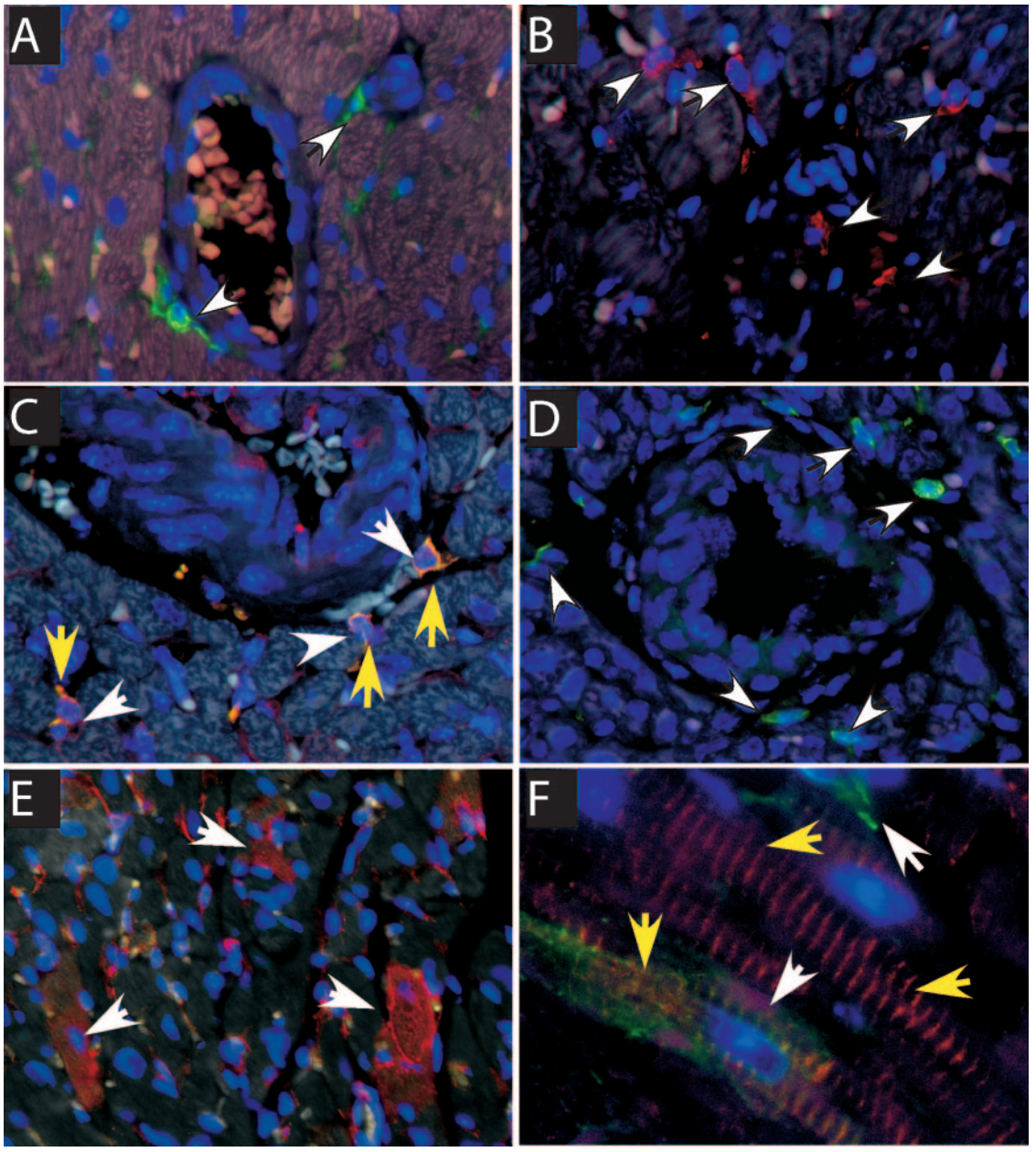

FIG. 2. Immunohistochemistry analysis of cell types in heart tissue. (A) Virus envelope protein (green fluorescence, white arrows) was detected on small cells located near blood vessels in Fr98-infected mice. (B) Macrophages were detected by Iba1 staining (red fluorescence, white arrows) near blood vessels in the heart. (C) Dual staining for virus envelope protein (red, white arrows) and macrophage marker Iba1 (green fluorescence, yellow arrows) show virus-infected macrophages (yellow fluorescence) in the heart. (D) XPR1-expressing cells in heart tissue. (E) Detection of virus envelope protein (red fluorescence) in multiple cells of the heart, including myocytes (white arrows). (F) Colocalization of virus envelope (green fluorescence, white arrows) and desmin (red fluorescence, yellow arrows) demonstrate virus infection of myocytes. Heart tissue from uninfected or Fr98-infected mice was removed at 18 to 21 dpi and processed for immunohistochemistry as described in Materials and Methods. Images were captured using Image Pro Plus 5.0 software. Magnification, ×200 (A, B, C, and D), ×100 (E), and ×1,000 (F).

cells appeared to be undergoing apoptosis based on nuclear morphology (Fig. 3C).

As the infection of myocytes was surprising, we analyzed heart tissue for the expression of the virus receptor XPR1. Multiple XPR1-positive cells were detected around blood vessels in the heart, indicating the expression of XPR1 on macrophages (Fig. 2D). However, myocytes were not positive for the receptor by immunohistochemistry. We then examined whether other muscle tissue was infected by the virus. No positive cells were detected in skeletal muscle from Fr98- or Fr54-infected mice (data not shown).

Lack of significant fibrosis in heart tissue from Fr98-infected mice. Viral infection in the heart can be associated with pathology that includes diffuse to marked lymphocytic infiltration, apoptosis of cardiomyocytes, and/or fibrosis (4, 6, 8, 14). Apoptotic cells were detectable in heart tissue from Fr98-

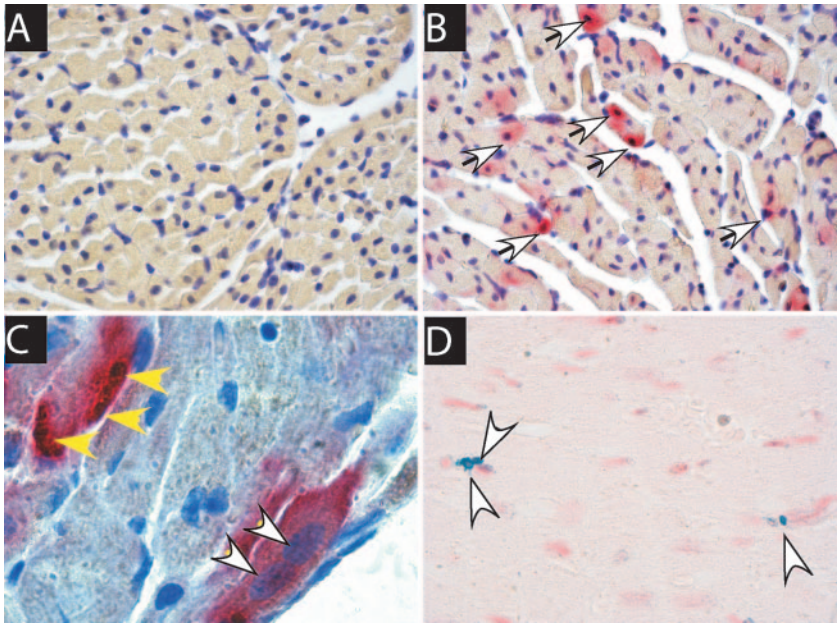

FIG. 3. (A to C) Confirmation of virus infection of myocytes by detection of viral RNA (red stain, white arrows) in myocytes. DIG-labeled RNA probe specific for the virus envelope gene was used to detect Fr98 viral RNA in (A) uninfected or (B and C) Fr98-infected mice. (D) Detection of TUNEL-positive apoptotic cells (blue nuclei, white arrows) near left ventricles of Fr98-infected mice. No TUNEL-positive cells were detected in heart tissue from uninfected or Fr54-infected mice. Heart tissue from uninfected or Fr98-infected mice was removed at 18 to 21 dpi and processed for in situ hybridization as described in Materials and Methods. Sections were counterstained with (A to C) hematoxylin or (D) neutral red. Images were captured using Image Pro Plus 5.0 software. Magnification, ×100 (A and B), ×1,000 (C), and ×100 (D).

infected mice at 3 wpi by staining with terminal deoxynucleotidyltransferase-mediated dUTP-biotin nick end labeling (TUNEL) (Fig. 3D) and were not present in either uninfected or Fr54-infected mice (data not shown). However, less than 25 apoptotic cells were detected per cross-sectional tissue section, suggesting that virus infection of myocytes did not result in substantial apoptosis of cardiomyocytes or destruction of tissue. Mild fibrosis was detected in some heart tissue samples, as determined by trichrome staining, but was not consistent in Fr98-infected mice (data not shown). The lack of consistent fibrosis correlated with a lack of increased α type 1 collagen (*Col1a1*) mRNA expression in heart tissue from Fr98-infected mice (Fig. 4A). Thus, Fr98 infection does not lead to substantial apoptosis and fibrosis in the heart.

Increased macrophage infiltration in heart tissue following Fr98 infection. Inflammatory lesions were not consistently detected in heart tissue from Fr98 mice, with a few regions of mild inflammatory infiltrate detected in hematoxylin-and-eosin-stained tissue sections from a small percentage of Fr98-infected mice at 3 wpi (data not shown). However, mRNA expression of the macrophage marker *F4/80* was significantly increased in heart tissue from Fr98-infected mice at 3 wpi, compared to that from uninfected or Fr54-infected mice (Fig. 4B). This finding suggested an increased presence of macrophages in the heart tissue in Fr98-infected mice, even in the absence of marked inflammation. No consistent increase in *Cd3* mRNA expression was observed in heart tissue, in agreement with the lack of consistent lymphocytic infiltration in the heart (data not shown).

Increased expression of cytokine genes/proteins in heart tissue following Fr98 infection. Increased expression of proinflammatory cytokines is often associated with cardiac disease (1, 5, 18, 35, 36). Quantitative real-time PCR analysis was used to determine whether specific cytokines or chemokines were upregulated by Fr98 infection compared to either Fr54-infected or uninfected controls. Chemokine ligand 5 (*Ccl5*/*RANTES*) mRNA expression was increased significantly in Fr98-infected mice as early as 1 wpi and remained high at 3 wpi (Fig. 4F). *Ccl4* (macrophage inflammatory protein 1β [MIP-1β]) mRNA was upregulated at 1 wpi, but was not increased at either 2 or 3 wpi (Fig. 4E). Beta interferon (Fig. 4C) and interleukin-1α (*Il-1α*) (data not shown) mRNA were not upregulated at the early days of infection, but they were significantly increased in Fr98-infected mice at 3 wpi. The expression of mRNA for other cytokines and chemokines, including gamma interferon (Fig. 4D), tumor necrosis factor (*Tnf*), and *Ccl33* (MIP-1α) (data not shown), either were not upregulated consistently by Fr98 infection or were upregulated to the same level by Fr98 and Fr54 infection. Thus, Fr98 infection did induce the upregulation of mRNA for specific cytokines and chemokines in the heart. Inducible nitric oxide synthetase, which is upregulated in other models of virus-induced myocarditis (10, 33), was only slightly upregulated in Fr98-infected mice at 2 wpi.

Heart tissue at 3 wpi was also analyzed for cytokine proteins by multiplex bead array. Similar to mRNA analysis, CCL5 was significantly upregulated in the hearts of Fr98-infected mice compared to that in the hearts of uninfected or Fr54-infected mice (Fig. 5B). CCL2 protein was also upregulated in the hearts of Fr98-infected mice (Fig. 5A). IL-12p70, CCL3, CCL4, and TNF protein were below detectable levels by multiplex bead array (data not shown). Thus, Fr98 infection of the

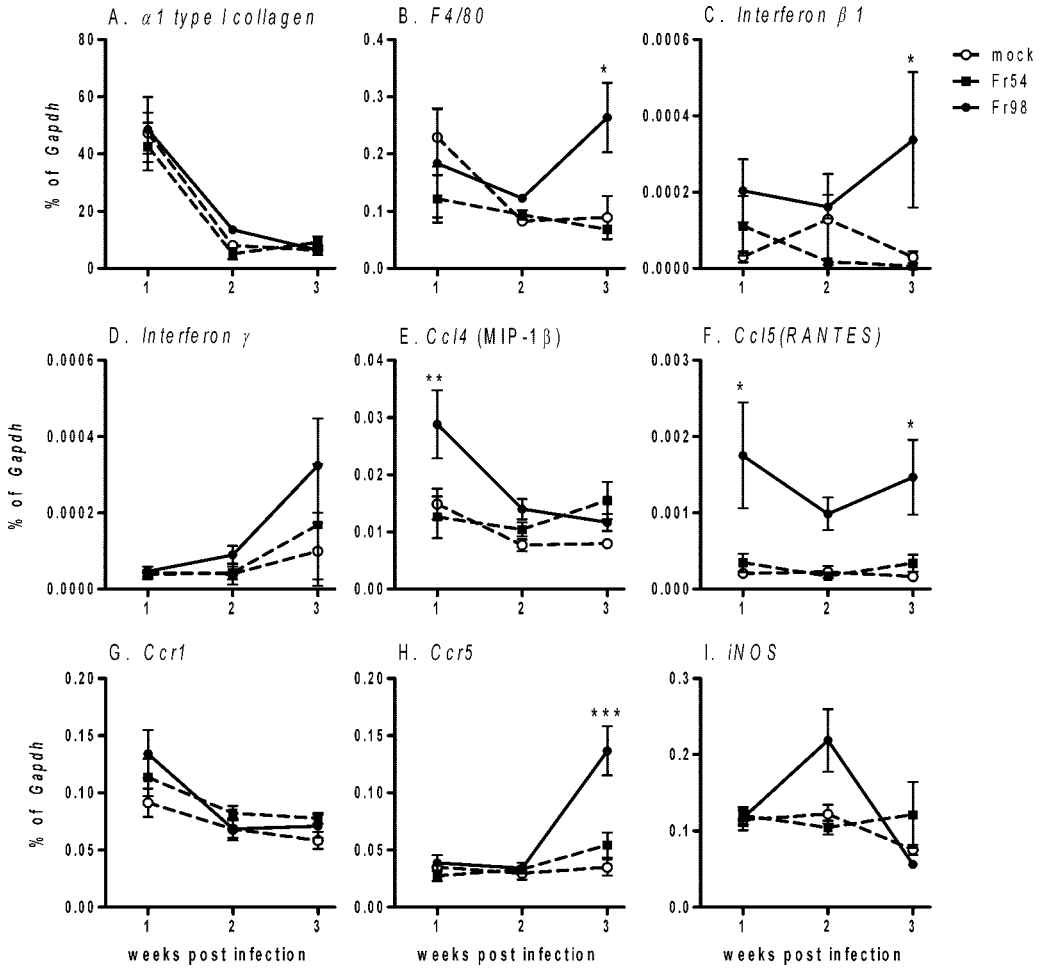

FIG. 4. mRNA expression of (A) α type 1 collagen, (B) F4/80, (C) beta 1 interferon, (D) gamma interferon, (E) *Ccl4*, (F) *Ccl5*, (G) *Ccr1*, (H) *Ccr5*, and (I) *iNos* in heart tissue of Fr98-infected, Fr54-infected, or uninfected 129SvEv mice. Newborn mice were infected with 10^4 focus-forming units of Fr98 or Fr54 by intraperitoneal injection. Heart tissue was removed from Fr98- and Fr54-infected mice at the indicated time, divided into two cross-sectional pieces, and snap-frozen in liquid nitrogen. mRNA levels were determined by using quantitative real-time PCR using SYBR green detection. Data were calculated as a percentage of *Gapdh* mRNA for each sample. Data are shown as the means ± standard errors (error bars) for four to seven samples per group per time point. Statistics were calculated using a two-way analysis of variance with Bonferroni's posttest. *, $P < 0.05$.

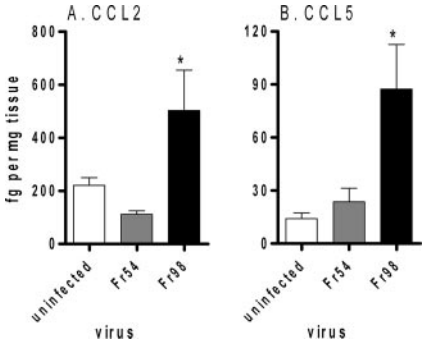

FIG. 5. Protein expression of CCL2 and CCL5 in heart tissue from uninfected, Fr54-infected, and Fr98-infected mice. Mice were infected as described for Fig. 3. Heart tissue was homogenized in lysis buffer and analyzed for protein expression by mutliplex bead array. Data were calculated as femtograms of chemokine per milligram of tissue homogenate. Data are shown as the means ± standard errors (error bars) of five mice per group. Statistical analysis was completed using a one-way analysis of variance with a Newman-Keul's posttest. *, $P < 0.05$.

heart induces a limited level of proinflammatory cytokines and chemokines that include CCL2 and CCL5, but not CCL3, CCL4, IL-12p70, or TNF protein.

Heart tissues were also examined to determine whether chemokine receptor expression was altered by Fr98 infection. Interestingly, *Ccr5* mRNA was upregulated at 3 wpi in Fr98-infected mice (Fig. 4H). The increase in *Ccr5* mRNA, which is expressed by macrophages, correlated with the increase in *F4/80* mRNA expression (Fig. 4B). Possibly, the increase in *Ccr5* mRNA is due to an influx of macrophages in the heart in response to the increased levels of CCL5.

Left ventricle dysfunction in 129SvEv mice infected with Fr98. To examine whether polytropic retrovirus infection induced measurable cardiac dysfunction, 129SvEv mice infected with Fr54 or Fr98 or uninfected controls were analyzed by echocardiogram at 3 wpi, the time frame in which Fr98-infected mice develop clinical signs of neurological disease. Mice were analyzed for the percentage of fractional shortening, a common measurement of left ventricle dysfunction (21, 26,

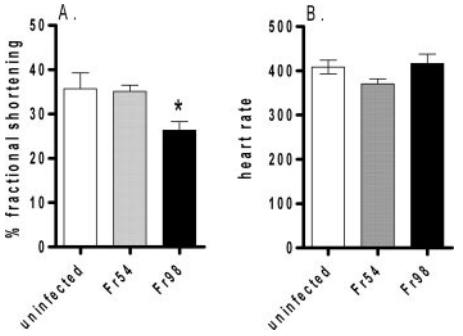

FIG. 6. Echocardiogram analysis of left ventricular dysfunction in Fr98-infected mice. (A) Mean percentage of fractional shortening from Fr98-infected, Fr54-infected, or uninfected mice at 3 wpi (18 to 25 days postinfection). Data are the means ± standard errors (error bars) of six to nine mice per group and are the combined results from three separate experiments. (B) Mean heart rates of Fr98-infected, Fr54-infected, and uninfected mice at 3 wpi (18 to 25 days). Data are the means ± standard errors (error bars) of three to seven mice per group. *, $P < 0.05$.

29). A significant decrease in the percentage of fractional shortening was observed for Fr98-infected mice compared to that for uninfected controls and Fr54-infected mice (Fig. 6A), indicating that Fr98 virus infection leads to cardiac dysfunction. No difference was observed in heart rate between any of the groups (Fig. 6B). Earlier kinetic studies of heart function were not possible due to the sizes of 1- to 2-week-old mice. Additionally, as the Fr98-infected mice developed severe clinical disease at 3 to 4 wpi, it was not possible to examine them at further time points.

No difference in the percentage of fractional shortening was detected between Fr54-infected mice and the uninfected controls at 3 wpi (Fig. 6A). As Fr54 virus does not induce severe neurological disease, we examined Fr54-infected mice and uninfected controls for cardiac dysfunction over a 3-month period. No difference in the percentage of fractional shortening was detected between Fr54 and uninfected controls over this time period (data not shown). Thus, Fr54 did not appear to induce cardiac damage.

Cardiac hormones, such as atrial natriuretic peptide and brain natriuretic peptide, which regulate water and electrolyte homeostasis, are upregulated in patients with chronic myocarditis but not acute myocarditis (38). No difference in *Anp* or *Bnp* mRNA was observed in heart tissue from Fr98-infected mice compared to heart tissue from uninfected or Fr54-infected mice (data not shown). This result suggested that Fr98 infection in the heart was not sufficient to induce significant changes in gene regulation of cardiac hormones in the heart.

DISCUSSION

In the current study, Fr98 retrovirus was found to infect cardiomyocytes and macrophages in the heart and induce left ventricular dysfunction (Fig. 2 and 6). Fr54 also infected the heart, but to a much lesser extent, and did not induce pathogenesis in the heart (Fig. 1 and 6 and data not shown). The pathogenesis induced by Fr98 infection was not associated with significant lymphocytic inflammation or fibrosis in the heart, but was associated with an increase in *F4/80*, *Ifnb1*, *Ccl5*, and *Ccr5* mRNA expression as well as CCL2 and CCL5 protein expression (Fig. 4 and 5). Thus, proinflammatory responses as well as direct virus infection may contribute to left ventricle dysfunction.

The kinetics of viral *gag* RNA expression differed substantially between the heart and the brain. In the brain, virus RNA levels were low at 1 wpi, but they increased logarithmically by 2 wpi to reach levels similar to those observed in the heart (Fig. 1). In contrast, at 1 wpi virus RNA levels were roughly 10-fold higher in the heart, but the levels increased only at a linear rate over the next 2 weeks. This result suggests two different mechanisms of virus spread. In the brain, virus infection is restricted around blood vessels early after infection and then spreads away from these blood vessels by virus-infected microglia and macrophages (27, 32). In the heart, virus infection was scattered throughout the heart, with a similar numbers of virus-infected cells at 1 wpi and 3 wpi as detected by in situ hybridization (data not shown). This finding suggests that the cells in the heart are infected with virus early on and that the virus does not spread between cells. Possibly, myocytes can be infected only within a certain time frame, thus preventing spread of virus after 1 wpi. The small increase in viral RNA in the heart between 2 to 3 wpi may be the recruitment of virus-infected macrophages to the heart.

Only a small number of cells were positive for apoptosis in Fr98-infected heart tissue, as detected by TUNEL staining (Fig. 3D). Thus, cardiomyocyte apoptosis does not appear to be a primary mechanism of Fr98-induced cardiac dysfunction. Technical difficulties prevented detection of the colocalization of apoptotic cells. The number of virus-infected cardiomyocytes per section was substantially greater than the number of apoptotic cardiomyocytes per section. Thus, Fr98 infection of cardiomyocytes did not correlate directly with myocyte apoptosis, although a few virus-infected cells had the appearance of condensed fragmented nuclei (Fig. 3C). No apoptotic cells were detected in Fr54-infected mice despite virus infection (data not shown). Thus, persistent retrovirus infection of cardiomyocytes in vivo does not appear to be detrimental to this cell type.

In patients with viral myocarditis, the primary pathology is generally patchy inflammation of lymphocytes and macrophages as well as some necrosis of myocytes (6, 8). The mouse model of Coxsackie B3 virus and mouse herpes virus-induced myocarditis are associated with patchy inflammatory infiltrate of lymphocytes in the heart, suggesting the involvement of the adaptive immune response (10, 13, 28, 33). The inflammatory response to Fr98 retrovirus infection in the heart is not associated with a strong lymphocytic infiltrate, but instead is more associated with macrophage infiltration. This finding suggests that the innate, rather than adaptive, immune response may play a more prominent role in Fr98 pathogenesis.

The lack of substantial lymphocytic inflammation in the heart tissue of Fr98-infected mice was surprising, considering the amount of virus present. Possibly, the neonatal age at which the mice are infected limits the development of a strong adaptive response and subsequent inflammation of the heart tissue. Endogenous retroviral sequences may also limit the availability of virus-specific epitopes for immune recognition (12, 20). The lack of detectable lymphocytic infiltrate may also

explain the lack of substantial fibrosis as the cardiomyocytes are not being destroyed by cytotoxic T lymphocytes.

Cytokines produced by lymphocytes or other infiltrating cells may play an important role in viral myocarditis. The production of multiple cytokines, including TNF and IFN-γ, as well as increased iNOS levels are associated with Coxsackie B3 virus-induced damage to the heart (10, 33). Furthermore, the injection of lipopolysaccharide induces left ventricle dysfunction and this response is associated with increased production of proinflammatory cytokines in the heart (22). Recent studies demonstrated that the constitutive production of IFN-γ in serum alone can result in inflammation, fibrosis, and/or atrophy of the heart muscle (30). Our present data with polytropic retrovirus infection did not demonstrate a consistent increase in TNF or IFN-γ levels in the heart (Fig. 4), possibly due to the lack of infiltrating T cells. However, other cytokines and chemokines, including CCL2, CCL5, and IFN-β, were upregulated in response to Fr98 and correlated with left ventricle dysfunction (Fig. 4, 5, and 6). Thus, these proinflammatory factors may contribute to left ventricle dysfunction.

Increased expression of *Ccl5* mRNA was detected in heart tissue of Fr98-infected mice at all time points analyzed (Fig. 4F). Interestingly, one of the receptors for CCL5, CCR5, was also upregulated in the heart, although only at 3 wpi (Fig. 4H). The increased expression of CCR5 correlated with increased expression of the macrophage marker F4/80 (Fig. 4B). Possibly, CCL5 production recruited CCR5-expressing macrophages to the heart. CCR5 has been shown to contribute to pathogenesis in other models of heart disease, including autoimmune myocarditis and *Trypanosoma cruzi*-induced myocarditis (11, 19), suggesting that it may also play a role in Fr98 pathogenesis.

ACKNOWLEDGMENTS

We thank Susan Pourciau and Marilyn Dietrich for technical assistance and critical readings of the manuscript and Larry Lomax for histological analysis of heart tissue.

This work was supported in part by National Center for Research Resources grant IP20RR020159.

REFERENCES

1. **Aukrust, P., T. Ueland, F. Muller, A. K. Andreassen, I. Nordoy, H. Aas, J. Kjekshus, S. Simonsen, S. S. Froland, and L. Gullestad.** 1998. Elevated circulating levels of C-C chemokines in patients with congestive heart failure. Circulation **97:**1136–1143.
2. **Beck, M. A., N. M. Chapman, B. M. McManus, J. C. Mullican, and S. Tracy.** 1990. Secondary enterovirus infection in the murine model of myocarditis. Pathologic and immunologic aspects. Am. J. Pathol. **136:**669–681.
3. **Beischel, J., D. F. Larson, Q. Yu, B. Yang, R. T. Sepulveda, T. Kelley, and R. R. Watson.** 2004. Dilated cardiomyopathy in retrovirally infected mice: a novel model for silent viral DCM? Cardiovasc. Toxicol. **4:**317–325.
4. **Bowles, N. E., D. L. Kearney, J. Ni, A. R. Perez-Atayde, M. W. Kline, J. T. Bricker, N. A. Ayres, S. E. Lipshultz, W. T. Shearer, and J. A. Towbin.** 1999. The detection of viral genomes by polymerase chain reaction in the myocardium of pediatric patients with advanced HIV disease. J. Am. Coll. Cardiol. **34:**857–865.
5. **Buzás, K., K. Megyeri, M. Hogye, M. Csanady, G. Bogats, and Y. Mandi.** 2004. Comparative study of the roles of cytokines and apoptosis in dilated and hypertrophic cardiomyopathies. Eur. Cytokine Netw. **15:**53–59.
6. **Calabrese, F., E. Rigo, O. Milanesi, G. M. Boffa, A. Angelini, M. Valente, and G. Thiene.** 2002. Molecular diagnosis of myocarditis and dilated cardiomyopathy in children: clinicopathologic features and prognostic implications. Diagn. Mol. Pathol. **11:**212–221.
7. **Chaves, A. A., M. J. Mihm, B. L. Schanbacher, A. Basuray, C. Liu, L. W. Ayers, and J. A. Bauer.** 2003. Cardiomyopathy in a murine model of AIDS: evidence of reactive nitrogen species and corroboration in human HIV/AIDS cardiac tissues. Cardiovasc. Res. **60:**108–118.
8. **Cioc, A. M., and G. J. Nuovo.** 2002. Histologic and in situ viral findings in the myocardium in cases of sudden, unexpected death. Mod. Pathol. **15:**914–922.
9. **Corbin, M. E., S. Pourciau, T. W. Morgan, M. Boudreaux, and K. E. Peterson.** 2006. Ligand up-regulation does not correlate with a role for CCR1 in pathogenesis in a mouse model of non-lymphocyte mediated neurological disease. J. Neurovirol. **12:**241–250.
10. **Fuse, K., G. Chan, Y. Liu, P. Gudgeon, M. Husain, M. Chen, W. C. Yeh, S. Akira, and P. P. Liu.** 2005. Myeloid differentiation factor-88 plays a crucial role in the pathogenesis of Coxsackievirus B3-induced myocarditis and influences type I interferon production. Circulation **112:**2276–2285.
11. **Gong, X., H. Feng, S. Zhang, Y. Yu, J. Li, J. Wang, and B. Guo.** 2007. Increased expression of CCR5 in experimental autoimmune myocarditis and reduced severity induced by anti-CCR5 monoclonal antibody. J. Mol. Cell. Cardiol. **42:**781–791.
12. **Gourley, M. F., W. J. Kisch, C. F. Mojcik, L. B. King, A. M. Krieg, and A. D. Steinberg.** 1992. Molecular aspects of systemic lupus erythematosus: murine endogenous retroviral expression. DNA Cell Biol. **11:**253–257.
13. **Hausler, M., B. Sellhaus, S. Scheithauer, B. Gaida, S. Kuropka, K. Siepmann, A. Panek, W. Berg, A. Teubner, K. Ritter, and M. Kleines.** Myocarditis in newborn wild-type BALB/c mice infected with the murine gamma herpesvirus MHV-68. Cardiovasc. Res., in press.
14. **Herskowitz, A., T. C. Wu, S. B. Willoughby, D. Vlahov, A. A. Ansari, W. E. Beschorner, and K. L. Baughman.** 1994. Myocarditis and cardiotropic viral infection associated with severe left ventricular dysfunction in late-stage infection with human immunodeficiency virus. J. Am. Coll. Cardiol. **24:**1025–1032.
15. **Iwasaki, T., N. Monma, R. Satodate, R. Kawana, and T. Kurata.** 1985. An immunofluorescent study of generalized Coxsackie virus B3 infection in a newborn infant. Acta Pathol. Jpn. **35:**741–748.
16. **Kearney, D. L., A. R. Perez-Atayde, K. A. Easley, N. E. Bowles, J. T. Bricker, S. D. Colan, S. Kaplan, W. W. Lai, S. E. Lipshultz, D. S. Moodie, G. Sopko, T. J. Starc, and J. A. Towbin, et al.** 2003. Postmortem cardiomegaly and echocardiographic measurements of left ventricular size and function in children infected with the human immunodeficiency virus. Cardiovasc. Pathol. **12:**140–148.
17. **Langston, C., E. R. Cooper, J. Goldfarb, K. A. Easley, S. Husak, S. Sunkle, T. J. Starc, and A. A. Colin.** 2001. Human immunodeficiency virus-related mortality in infants and children: data from the Pediatric Pulmonary and Cardiovascular Complications of Vertically Transmitted HIV (P^2C^2) Study. Pediatrics **107:**328–338.
18. **Lotan, D., D. Zilberman, O. Dagan, N. Keller, R. Ben-Abraham, A. A. Weinbroum, R. Harel, Z. Barzilay, and G. Paret.** 2001. Beta-chemokine secretion patterns in relation to clinical course and outcome in children after cardiopulmonary bypass: continuing the search to abrogate systemic inflammatory response. Ann. Thorac. Surg. **71:**233–237.
19. **Lubarsky, L., V. Jelnin, N. Marino, and H. S. Hecht.** 2007. Images in cardiovascular medicine. Caseous calcification of the mitral annulus by 64-detector-row computed tomographic coronary angiography: a rare intracardiac mass. Circulation **116:**e114–e115.
20. **Miyazawa, M., and R. Fujisawa.** 1994. Physiology and pathology of host immune responses to exogenous and endogenous murine retroviruses—from gene fragments to epitopes. Tohoku J. Exp. Med. **173:**91–103.
21. **Nemoto, S., G. DeFreitas, D. L. Mann, and B. A. Carabello.** 2002. Effects of changes in left ventricular contractility on indexes of contractility in mice. Am. J. Physiol. Heart Circ. Physiol. **283:**H2504–H2510.
22. **Nemoto, S., J. G. Vallejo, P. Knuefermann, A. Misra, G. DeFreitas, B. A. Carabello, and D. L. Mann.** 2002. Escherichia coli LPS-induced LV dysfunction: role of Toll-like receptor-4 in the adult heart. Am. J. Physiol. Heart Circ. Physiol. **282:**H2316–H2323.
23. **Peterson, K. E., J. S. Errett, T. Wei, D. E. Dimcheff, R. Ransohoff, W. A. Kuziel, L. Evans, and B. Chesebro.** 2004. MCP-1 and CCR2 contribute to non-lymphocyte-mediated brain disease induced by Fr98 polytropic retrovirus infection in mice: role for astrocytes in retroviral neuropathogenesis. J. Virol. **78:**6449–6458.
24. **Peterson, K. E., S. Hughes, D. E. Dimcheff, K. Wehrly, and B. Chesebro.** 2004. Separate sequences in a murine retroviral envelope protein mediate neuropathogenesis by complementary mechanisms with differing requirements for tumor necrosis factor alpha. J. Virol. **78:**13104–13112.
25. **Peterson, K. E., S. J. Robertson, J. L. Portis, and B. Chesebro.** 2001. Differences in cytokine and chemokine responses during neurological disease induced by polytropic murine retroviruses map to separate regions of the viral envelope gene. J. Virol. **75:**2848–2856.
26. **Pollick, C., S. L. Hale, and R. A. Kloner.** 1995. Echocardiographic and cardiac Doppler assessment of mice. J. Am. Soc. Echocardiogr. **8:**602–610.
27. **Portis, J. L., S. Czub, S. Robertson, F. McAtee, and B. Chesebro.** 1995. Characterization of a neurologic disease induced by a polytropic murine retrovirus: evidence for differential targeting of ecotropic and polytropic viruses in the brain. J. Virol. **69:**8070–8075.
28. **Rabin, E. R., S. A. Hassan, A. B. Jenson, and J. L. Melnick.** 1964. Coxsackie virus B3 myocarditis in mice. An electron microscopic, immunofluorescent and virus-assay study. Am. J. Pathol. **44:**775–797.
29. **Raidel, S. M., C. Haase, N. R. Jansen, R. B. Russ, R. L. Sutliff, L. W. Velsor, B. J. Day, B. D. Hoit, A. M. Samarel, and W. Lewis.** 2002. Targeted myo-

cardial transgenic expression of HIV Tat causes cardiomyopathy and mitochondrial damage. Am. J. Physiol. Heart Circ. Physiol. **282:**H1672–H1678.

30. **Reifenberg, K., H. A. Lehr, M. Torzewski, G. Steige, E. Wiese, I. Kupper, C. Becker, S. Ott, P. Nusser, K. Yamamura, G. Rechtsteiner, T. Warger, A. Pautz, H. Kleinert, A. Schmidt, B. Pieske, P. Wenzel, T. Munzel, and J. Lohler.** 2007. Interferon-γ induces chronic active myocarditis and cardiomyopathy in transgenic mice. Am. J. Pathol. **171:**463–472.
31. **Robertson, M. N., M. Miyazawa, S. Mori, B. Caughey, L. H. Evans, S. F. Hayes, and B. Chesebro.** 1991. Production of monoclonal antibodies reactive with a denatured form of the Friend murine leukemia virus gp70 envelope protein: use in a focal infectivity assay, immunohistochemical studies, electron microscopy and western blotting. J. Virol. Methods **34:**255–271.
32. **Robertson, S. J., K. J. Hasenkrug, B. Chesebro, and J. L. Portis.** 1997. Neurologic disease induced by polytropic murine retroviruses: neurovirulence determined by efficiency of spread to microglial cells. J. Virol. **71:**5287–5294.
33. **Robinson, N. M., H. Y. Zhang, A. L. Bevan, A. J. De Belder, S. Moncada, J. F. Martin, and L. C. Archard.** 1999. Induction of myocardial nitric oxide synthase by Coxsackie B3 virus in mice. Eur. J. Clin. Investig. **29:**700–707.
34. **Rozen, S., and H. J. Skaletsky.** 2000. Primer3 on the WWW for general users and for biologist programmers. Methods Mol. Biol. **132:**365–386.
35. **Satoh, M., M. Nakamura, G. Tamura, S. Makita, I. Segawa, A. Tashiro, R. Satodate, and K. Hiramori.** 1997. Inducible nitric oxide synthase and tumor necrosis factor-alpha in myocardium in human dilated cardiomyopathy. J. Am. Coll. Cardiol. **29:**716–724.
36. **Seino, Y., U. Ikeda, H. Sekiguchi, M. Morita, K. Konishi, T. Kasahara, and K. Shimada.** 1995. Expression of leukocyte chemotactic cytokines in myocardial tissue. Cytokine **7:**301–304.
37. **Tailor, C. S., A. Nouri, C. G. Lee, C. Kozak, and D. Kabat.** 1999. Cloning and characterization of a cell surface receptor for xenotropic and polytropic murine leukemia viruses. Proc. Natl. Acad. Sci. USA **96:**927–932.
38. **Takemura, G., H. Fujiwara, Y. Takatsu, T. Fujiwara, and K. Nakao.** 1995. Venticular expression of atrial and brain natriuretic peptides in patients with myocarditis. Int. J. Cardiol. **52:**213–222.
39. **Twu, C., N. Q. Liu, W. Popik, M. Bukrinsky, J. Sayre, J. Roberts, S. Rania, V. Bramhandam, K. P. Roos, W. R. MacLellan, and M. Fiala.** 2002. Cardiomyocytes undergo apoptosis in human immunodeficiency virus cardiomyopathy through mitochondrion- and death receptor-controlled pathways. Proc. Natl. Acad. Sci. USA **99:**14386–14391.
40. **Yang, Y. L., L. Guo, S. Xu, C. A. Holland, T. Kitamura, K. Hunter, and J. M. Cunningham.** 1999. Receptors for polytropic and xenotropic mouse leukaemia viruses encoded by a single gene at Rmc1. Nat. Genet. **21:**216–219.
41. **Yearley, J. H., C. Pearson, R. P. Shannon, and K. G. Mansfield.** 2007. Phenotypic variation in myocardial macrophage populations suggests a role for macrophage activation in SIV-associated cardiac disease. AIDS Res. Hum. Retrovir. **23:**515–524.